

Magnetic layer thickness dependence of magnetization reversal in electrodeposited CoNi/Cu multilayer nanowires

Xue-Ti Tang^{a,*}, Gwo-Ching Wang^a, Mitsuhiro Shima^b

^a*Department of Physics, Applied Physics and Astronomy, Rensselaer Polytechnic Institute, Troy, NY 12180-3590, USA*

^b*Department of Materials Science and Engineering, Rensselaer Polytechnic Institute, Troy, NY 12180-3590, USA*

Received 25 March 2006; received in revised form 19 June 2006

Available online 21 July 2006

Abstract

The magnetization reversal of electrodeposited CoNi/Cu multilayer nanowires patterned in an array using a hole template has been investigated. The reversal mode is found to depend on the CoNi layer thickness $t(\text{CoNi})$; with increasing $t(\text{CoNi})$ a transition occurs from coherent rotation to a combination of coherent and incoherent rotation at around $t(\text{CoNi}) = 51$ nm. The reversal mode has been identified using the magnetic hysteresis loops measured at room temperature for CoNi/Cu nanowires placed at various angles between the directions of the nanowire axis and external fields using a vibrating sample magnetometer. The nanowire samples have a diameter of ~ 250 nm and constant Cu layer thickness of 4.2 nm with various $t(\text{CoNi})$ ranging from 6.8 nm to 7.5 μm . With increasing $t(\text{CoNi})$, the magnetic easy axis moves from the direction perpendicular to nanowires to that parallel to the nanowires at around $t(\text{CoNi}) = 51$ nm, indicating a change in the magnetization reversal mode. The reversal mode for the nanowires with thin disk-shaped CoNi layers ($t(\text{CoNi}) = 6.8, 12$ and 17 nm) is of a coherent rotation type, while that for long rod-shaped CoNi layers ($t(\text{CoNi}) = 150$ nm, 1.0, 2.5 and 7.5 μm) can be consistently explained by a combination of coherent rotation and a curling mode. The effects of dipole–dipole interactions between nanowires and between adjacent magnetic layers in each nanowire on the reversal process have been discussed.

© 2006 Elsevier B.V. All rights reserved.

PACS: 75.60.Jk; 75.75.+a; 75.70.Cn; 81.15.Pq

Keywords: Magnetic nanowire; Magnetic layered films; Magnetization reversal

1. Introduction

The increasing interest in nanostructured magnetic materials has been driven by demands for their practical applications as well as by their scientific importance in the last decades. Remarkable progress has been made on their technological applications, particularly for magnetic and spintronic devices such as high-density data storage and magnetic field sensors. Extensive studies have been performed on the unique magnetic properties of the nanostructured materials, with particular focus on the superparamagnetism in fine particles and the magnetization reversal mechanism. Among various nanoscale magnetic materials, magnetic/nonmagnetic multilayer

nanowires are of particular interest because of their unique magnetotransport properties in the confined geometry. Although the phenomenon known as giant magnetoresistance (GMR) effect in the current perpendicular to plane (CPP) geometry has been well studied in general [1–5], little has been understood in the magnetization reversal mechanism in the multilayer nanowire systems. As the experimental determination of the magnetization reversal mode for nanoscale magnetic objects remains as a challenge for decades, most work has been focused on the computational modeling [6–14]. A few models have been proposed for the magnetization reversal of nanoscale magnetic objects: coherent rotation, curling, buckling, fanning, and nucleation of reversed domains. In this study, the coherent rotation and curling models are considered for the magnetization reversal of the CoNi/Cu nanowires since these models are among the most suitable for

*Corresponding author. Tel.: +1 518 276 3362; fax: +1 518 276 6680.
E-mail address: tangx@rpi.edu (X.-T. Tang).

nanostructured magnetic objects, particularly nanowire systems [15,16]. The magnetization reversal by coherent rotation proceeds with all the spins in each magnet rotating in unison to maintain the exchange energy E_{ex} of the system minimum at the cost of increased magnetostatic energy E_{ms} [17]. The reversal process in the curling mode goes on with the spins in each magnet incoherently rotating in a curling pattern to maintain E_{ms} minimum at the cost of increased E_{ex} [18,19]. In general, magnetization reversal can be explained by considering the total energy of the system at minimum, where the total energy is given by the sum of E_{ex} and E_{ms} . The coherent rotation mode is more favorable when E_{ex} is minimized in the system, while the curling mode is more favorable when E_{ms} is minimized. Previously the magnetization reversal of magnetic particles and nanorods has been explained using the coherent rotation and curling models [15,16,20]. Multilayer nanowires indeed provide a unique opportunity to investigate the magnetization reversal mechanism since each magnetic layer in the multilayer can be formed in a desired shape as a disk or a rod simply by changing the layer thickness during the nanowire growth. Interlayer magnetostatic couplings are likely to reside in each multilayer nanowire. When nanowires are in proximity to the other nanowires, interwire magnetostatic couplings may also exist in the system. These interactions can also affect the magnetization reversal behavior of the multilayer nanowires.

The objective of this paper is to systematically study the magnetization reversal mechanism in CoNi/Cu multilayer nanowires as a function of the CoNi layer thickness $t(\text{CoNi})$. In the study, the magnetization reversal mode has been identified for samples with various $t(\text{CoNi})$ after taking into account the magnetostatic interactions between nanowires and between adjacent magnetic layers in each nanowire. The multilayer nanowires were grown into a nanoporous template using a single-bath electrodeposition technique.

2. Experimental

CoNi/Cu multilayer nanowires were grown by electrodeposition using a commercial alumina template (Anodisc[®]) which has an array of holes with the size of 60 μm in length and ~ 250 nm in diameter. A thin conducting layer of gold was coated on one side of each template that served as a working electrode for electrodeposition. An electrical contact was made to the conducting layer and masked using an insulating tape so that only holes on the other side of the template were exposed. The template was then submerged in an electrolytic solution containing 2.3 M $\text{Ni}(\text{SO}_3\text{NH}_2)_2$, 0.4 M CoSO_4 , 0.025 M CuSO_4 , and 0.5 M H_3BO_3 [21] with the pH value of 2.2. The electrodeposition cell consists of vertically positioned electrodes: a working electrode prepared in the method described above, a counter electrode made of platinum, and an Ag/AgCl reference electrode [5,22]. The multilayer nanowires were electrodeposited using a pulsed potential technique by

periodically switching the deposition potential between -0.2 and -1.0 V for deposition of the Cu and CoNi layers, respectively. The thickness of each layer was controlled by optimizing the pulse duration and the cumulative charge transferred during each pulse. The actual thickness of each layer was determined by visually examining the structure of the multilayer nanowires by scanning electron microscopy (SEM). In order to clearly identify the individual layers in the SEM images and to estimate their growth rate, multilayer nanowire samples with the thickness of each layer greater than that of the samples used for magnetic characterization were also prepared. The structure of the multilayer nanowires was also examined by X-ray diffraction (XRD) measurements. Prior to the XRD measurements, the alumina templates of the samples were etched partially using a 4 M NaOH solution in order to expose the nanowires to the X-ray beam, with overall alignment of the nanowires maintained.

Magnetic characterization of the nanowire samples was carried out without removing the alumina templates. The thickness of the CoNi layers $t(\text{CoNi})$ in the multilayer nanowires was varied in a range 6.8 nm–7.5 μm with the Cu layer thickness $t(\text{Cu})$ kept constant at 4.2 nm. To study the magnetization reversal mechanism of the CoNi/Cu nanowires, the magnetic hysteresis loops were measured at room temperature in an applied field of up to 12 kOe using a vibrating sample magnetometer (VSM) at various angles θ between the direction of the nanowire axis and the field ranging from 0° to 180° in steps of 15° .

3. Results and discussion

3.1. Structure of CoNi/Cu nanowires

The structure of CoNi/Cu multilayer nanowires was first examined using SEM. Figs. 1(a) and (b) show nanowires consisting of periodically alternating CoNi and Cu layers with thicknesses of $t(\text{CoNi}) = 36 \pm 4$ nm and $t(\text{Cu}) = 26 \pm 4$ nm, respectively. The purpose of imaging nanowires using a larger Cu layer thickness than those studied by VSM is to easily identify the Cu layers with the resolution of the SEM that we used. Prior to SEM imaging, the alumina template was mechanically broken. The nanowires partially exposed outside the template were imaged by scanning the cross-section of the broken template. Well-aligned nanowires with a diameter of ~ 250 nm are readily seen in the images, which are separated by a center-to-center spacing of ~ 450 nm from their adjacent nanowires. Figs. 1(c) and (d) show nanowires after the template was chemically removed using a NaOH solution before imaging. In this case, the nanowires are more irregularly distributed than those with the template, since the nanowires are relatively free to shift in the absence of support. Indeed, bundles of adjacent nanowires are readily observed with spacing smaller than ~ 450 nm (see Figs. 1(c) and (d)).

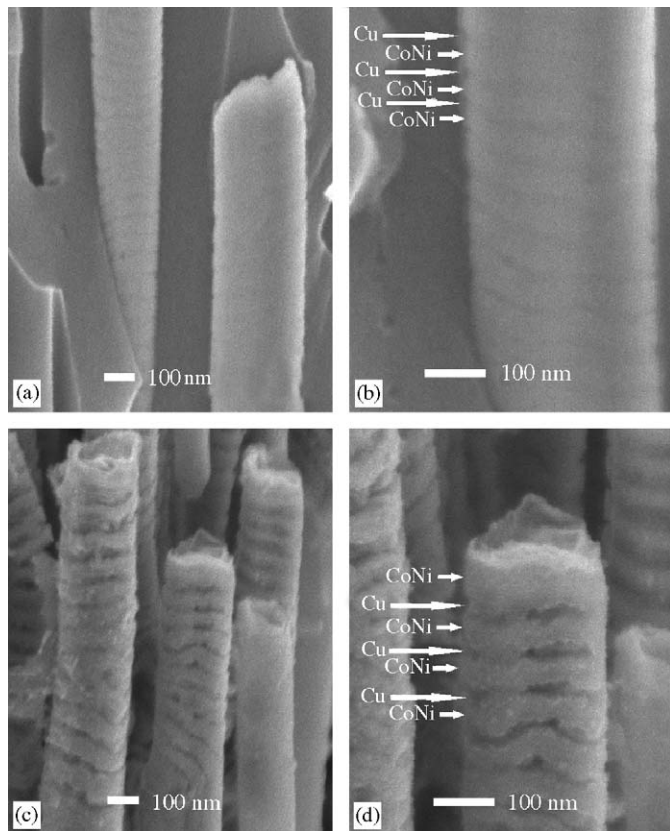


Fig. 1. SEM images of CoNi/Cu nanowires with layer thicknesses of $t(\text{CoNi}) = 36 \pm 4$ nm and $t(\text{Cu}) = 26 \pm 4$ nm. The images (a) and (b) were obtained at the magnification of (a) $\times 50,000$ and (b) $\times 100,000$ before the template was removed. The images (c) and (d) were taken at (c) $\times 50,000$ and (d) $\times 100,000$ after the template was removed.

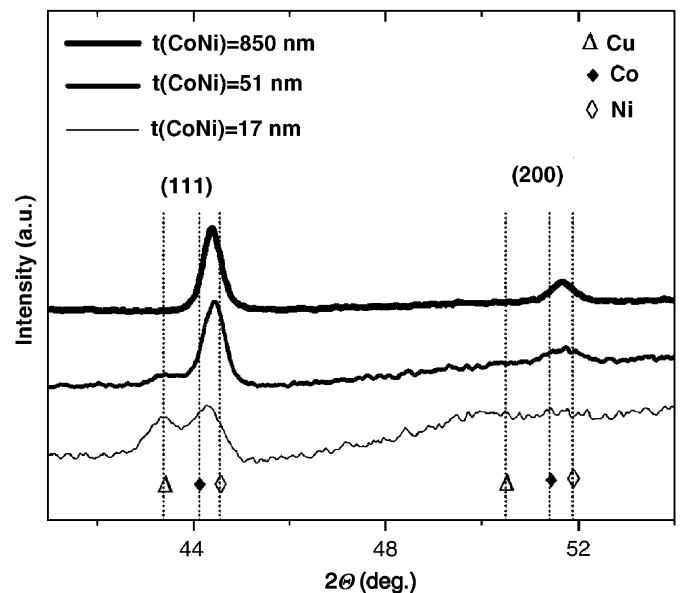


Fig. 2. XRD spectra for CoNi/Cu nanowires with $t(\text{Cu}) = 4.2$ nm and various $t(\text{CoNi}) = 850$, 51, and 17 nm. The vertical lines in the figure indicate the positions of the diffraction peaks for pure FCC-Cu (triangles), pure FCC-Co (filled circles), and FCC-Ni (open circles), estimated from their bulk lattice constants.

layers. Since the (111) peaks for Cu are separated from those for the CoNi layers, the lattice constant for the FCC-Cu in each sample is different from that for the FCC-CoNi, indicating that the multilayers are not pseudomorphically grown. Since the lengths of the nanowires for all the sample are kept constant at ~ 20 μm , the intensity ratio of the Cu (111) peak relative to that of CoNi decreases with increasing $t(\text{CoNi})$ and vanishes for $t(\text{CoNi}) = 850$ nm, due to the decrease in the total volume of Cu and the increase in that of CoNi in the sample. The intensity ratio of the CoNi (111) peak relative to the (200) peak is larger than that predicted for the polycrystalline alloy, indicating that the sample has a (111) texture along the direction of the nanowire axis, which strongly depends on $t(\text{CoNi})$. As shown in Fig. 2, the intensity ratio of the (111) peak relative to the (200) peak increases with decreasing $t(\text{CoNi})$, indicating an increase in the (111) texture. The (200) peak is evident for $t(\text{CoNi}) = 850$ nm, while it vanishes for $t(\text{CoNi}) = 17$ nm, implying that the (111) texture of the nanowires is enhanced by further decreasing $t(\text{CoNi})$.

3.2. Magnetic easy axis

The magnetic hysteresis loops were measured at room temperature for CoNi/Cu nanowires with various $t(\text{CoNi})$ in magnetic fields applied perpendicular and parallel to the nanowire axis. As $t(\text{CoNi})$ decreases, the easy axis of the nanowires changes from the direction parallel to nanowires to that perpendicular to the nanowires. The CoNi layers in the multilayer nanowires with $t(\text{CoNi}) = 7.5$, 2.5, and 1 μm , and 150 nm are formed in a rod-like shape. In this case, the

Fig. 2 shows XRD spectra measured in the θ - 2θ scan mode for CoNi(x)/Cu(4.2 nm) multilayer nanowires with CoNi layer thicknesses $x = 850$, 51, and 17 nm. Peaks are readily observed at $2\theta \sim 44^\circ$ and 52° which, respectively, correspond to the (111) and (200) Bragg reflections of the face-centered cubic (FCC) lattice, indicating that the structure of nanowires is FCC. No superlattice satellite peaks were observed in the spectra, presumably due to a thickness variation of the individual layers in the nanowires. Assuming that the CoNi alloy in the magnetic layers forms a solid solution, the lattice constant of the FCC-CoNi varies approximately linearly with composition of the alloy in the range between the values for pure FCC-Co and FCC-Ni. The corresponding peak positions for the CoNi layers in the X-ray spectra should change linearly with the alloy composition. Estimated from the (111) peak positions, the lattice constants for $t(\text{CoNi}) = 850$, 51 and 17 nm are 3.532 \AA , 3.530 \AA and 3.540 \AA , respectively. These values indeed fall in the range between those for FCC-Co (3.55 \AA) and FCC-Ni (3.52 \AA). Besides the peaks for CoNi, a separate peak is observed for samples with $t(\text{CoNi}) = 17$ nm and $t(\text{CoNi}) = 51$ nm at $2\theta \sim 43.4^\circ$, which is slightly lower than that for the (111) peak for CoNi ($2\theta \sim 44.3^\circ$), corresponding to the (111) peak for Cu

saturation field measured along the nanowire axis ($\theta = 0^\circ$) is smaller than that for the directions perpendicular to the axis ($\theta = 90^\circ$), indicating that the magnetic easy axis lies in the direction parallel to the nanowires, as shown in Fig. 3. The CoNi layers in the nanowires with $t(\text{CoNi}) = 17, 12$ and 6.8 nm have a thin-disk shape. In this case, the magnetic easy

axis lies in the direction perpendicular to the nanowires, as shown in Fig. 4. A transition for the direction of the magnetic easy axis occurs at about $t(\text{CoNi}) = 51 \pm 6$ nm, which corresponds to a ratio of $t/d = 0.2$, where t and d , respectively, represent the thickness of the CoNi layers and the diameter of the nanowires (~ 250 nm).

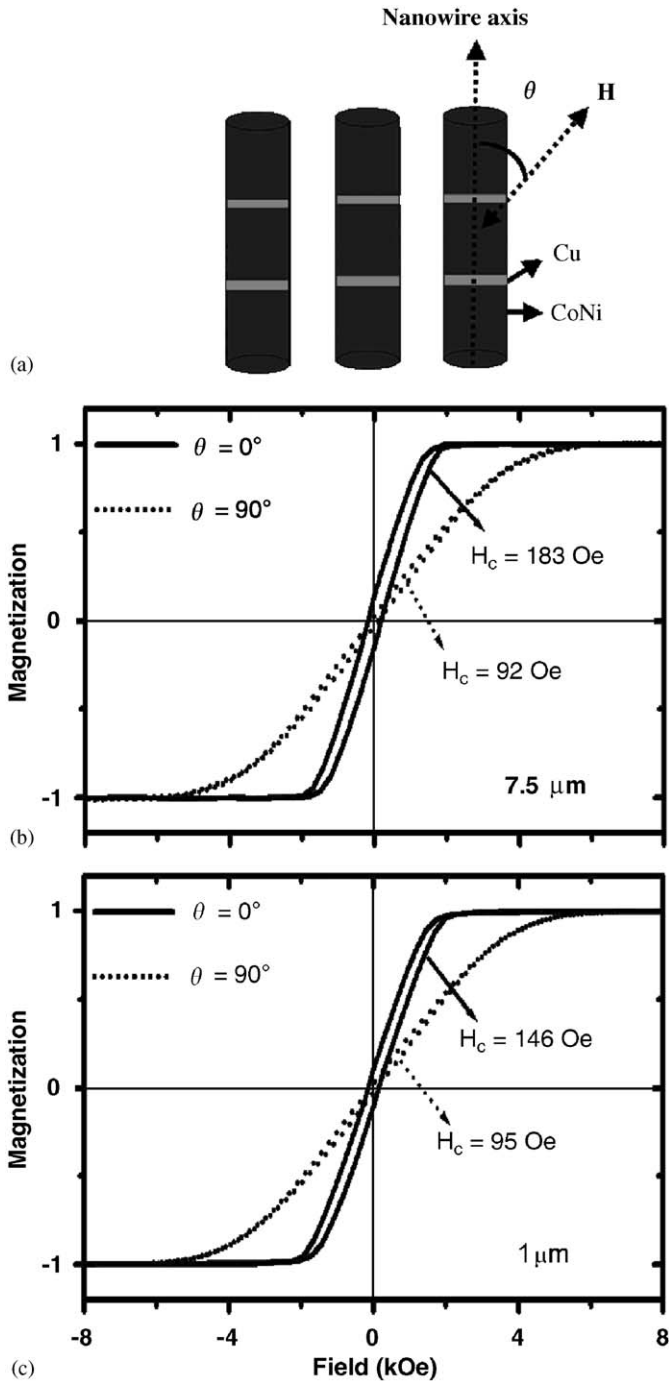


Fig. 3. (a) Schematic representation showing the geometry of multilayer nanowires, applied magnetic field H , and the angle θ between them, (b) room-temperature magnetic hysteresis loops measured for CoNi/Cu nanowires with $t(\text{Cu}) = 4.2$ nm and $t(\text{CoNi}) = 7.5 \mu\text{m}$, and (c) room-temperature hysteresis loops for CoNi/Cu nanowires with $t(\text{Cu}) = 4.2$ nm and $t(\text{CoNi}) = 1 \mu\text{m}$.

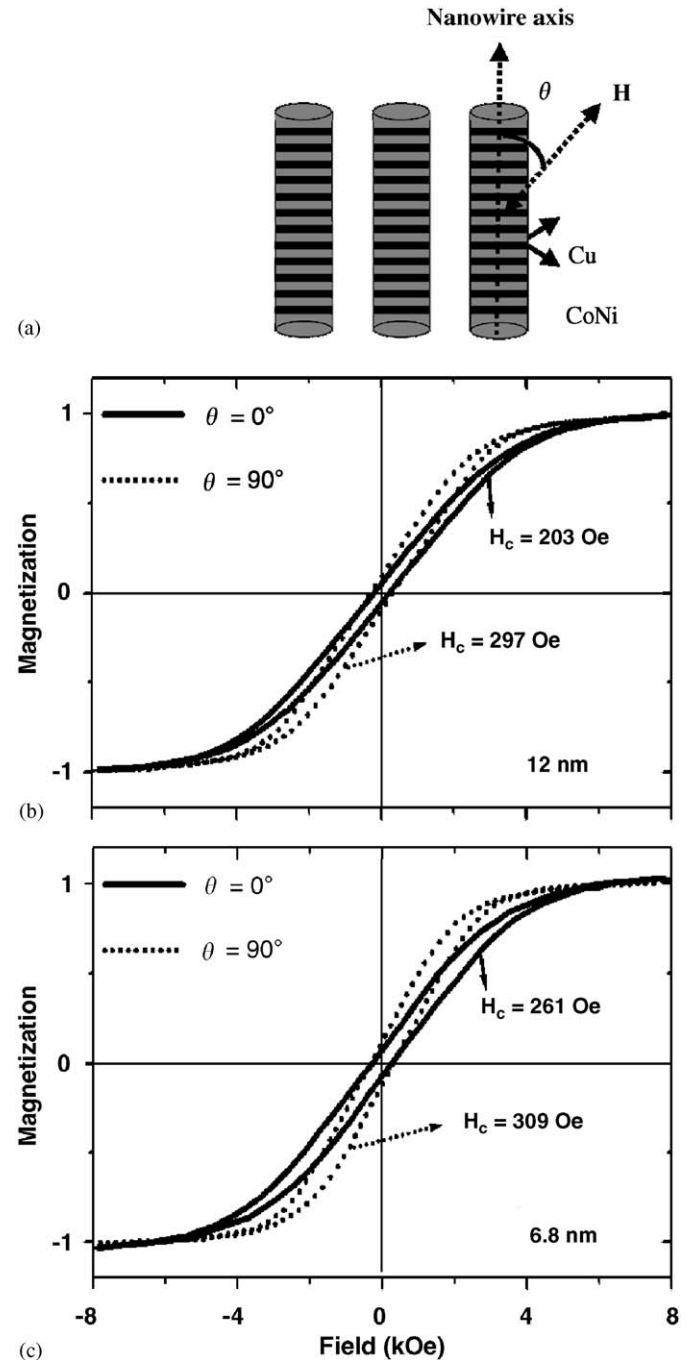


Fig. 4. (a) Schematic representation showing the geometry of multilayer nanowires, applied magnetic field H , and the angle θ between them, (b) room-temperature magnetic hysteresis loops measured for CoNi/Cu nanowires with $t(\text{Cu}) = 4.2$ nm and $t(\text{CoNi}) = 12$ nm, and (c) room-temperature hysteresis loops for CoNi/Cu nanowires with $t(\text{Cu}) = 4.2$ nm and $t(\text{CoNi}) = 6.8$ nm.

Since the value $t/d = 0.2$ for the transition is much smaller than $t/d = 1$, the shape anisotropy is not negligible so that both the magnetocrystalline anisotropy and shape anisotropy should be considered in evaluating the direction of the magnetic easy axis. As discussed in Section 3.1, the CoNi layers have a (1 1 1) texture along the nanowires. As both pure FCC-Co and FCC-Ni are known to have an easy axis along the $\langle 111 \rangle$ direction, it is reasonable to assume that the easy axis of FCC-CoNi also lies in the $\langle 111 \rangle$ direction. It is therefore suggested that the magnetocrystalline anisotropy of the (1 1 1)-textured CoNi layers tends to have the easy axis along the nanowire axis. When $t/d > 1$, the easy axis lies along the nanowire axis since both the shape anisotropy and magnetocrystalline anisotropy tend to align the easy axis along the nanowires. When $1 > t/d > 0.2$, the easy axis actually lies along the nanowire axis even though the shape anisotropy is expected to align it perpendicular to the nanowire axis, probably because the magnetocrystalline anisotropy is more dominant than the shape anisotropy in this range. When $t/d < 0.2$, the easy axis lies in the direction perpendicular to the nanowires because shape anisotropy dominates over magnetocrystalline anisotropy in this range of the aspect ratio.

3.3. Magnetic dipole interactions between nanowires and between layers

Besides the magnetocrystalline anisotropy and shape anisotropy in the magnetic layers described in Section 3.2, the dipole–dipole interactions between nanowires H_{Dipole} can also affect the magnetization process and the magnetic easy axis of magnetic nanowires [23–30]. Previously, Zhan et al. [30] have shown that a sizable dipole–dipole interaction can be induced between nanowires when an external magnetic field H_{ex} is applied perpendicular to the nanowire axis, while the interaction may be negligibly small when H_{ex} is applied along the nanowire axis. When H_{ex} is perpendicular to the nanowire axis, H_{Dipole} is parallel to H_{ex} so that a smaller external field is required to saturate the magnetization of the nanowires for the magnetic hysteresis loop measurement. For the multilayer nanowires with magnetic layers in a rod shape, it is possible to change the direction of the easy axis from the direction parallel to the nanowires to that perpendicular to the nanowires by increasing H_{Dipole} . As described in Section 3.2, the CoNi/Cu nanowires with $t/d > 1$ maintain their easy axis parallel to the nanowires. In this case, H_{Dipole} may not be large enough to re-orient the easy axis to the direction perpendicular to the nanowires. As we previously reported [5], the effect of magnetocrystalline anisotropy may be negligible compared to the shape anisotropy, as shown in the reduced (1 1 1) texture of the CoNi/Cu nanowires with larger t (CoNi). The relatively weak H_{Dipole} is probably due to the relatively large center-to-center spacing between nanowires (~ 450 nm) as shown in Figs. 1(a) and (b). H_{Dipole} induced by H_{ex} perpendicular to the nanowire axis can be approximately calculated using the formula given by Zhan

et al. [30]; $H_{\text{Dipole}} = 1.379\pi^2 M(d/d_{\text{ww}})^2$, where M and d_{ww} are, respectively, the magnetization of the nanowires and the spacing between nanowires. The calculated value for H_{Dipole} is ~ 4000 Oe for the CoNi/Cu nanowires. The self-demagnetizing field H_{Dem} for a nanowire under a field applied perpendicular to the nanowire is $2\pi M \sim 6000$ Oe for the nanowires, which is larger than H_{Dipole} . This simple estimation consistently explains the result obtained for $t/d > 1$, where the easy axis lies along the nanowire axis.

The magnetic anisotropy for $t/d > 1$ is strong, as indicated by the large difference in the saturation field between the directions perpendicular and parallel to the nanowires. In this case, the dipole–dipole interaction between adjacent CoNi layers tends to align the magnetization of the layers along the nanowire axis with different poles facing each other. The magnetic behavior of a multilayer nanowire resembles that of a single-element magnetic nanowire that tends to have a strong shape anisotropy due to the elongated shape. On the other hand, the magnetic anisotropy for thin disk-shaped CoNi layers is weak, as indicated by a very small difference in saturation fields between the directions perpendicular and parallel to the nanowire axis. The disk-shaped CoNi layers are expected to have a predominant shape anisotropy that tends to align the easy axis in the disk plane. The shape anisotropy could be much stronger than the magnetocrystalline anisotropy [5]. The actual in-plane anisotropy within the multilayer nanowires is weaker than the predicted value maybe because there exists dipole–dipole interactions between adjacent CoNi layers in each nanowire [31]. For multilayer nanowires with magnetic layers formed in a disk shape, the dipole–dipole interactions between adjacent magnetic layers tend to induce an antiparallel alignment of magnetization oriented perpendicular to the nanowire axis [31]. It should be noted that RKKY exchange coupling does not induce the antiparallel alignment of magnetization in our sample because the Cu layer thickness of 4.2 nm is too large for RKKY coupling to play a major role. When a magnetic field is applied perpendicular to the nanowires (i.e., parallel to the CoNi layers), magnetization reversal can be achieved when the field exceeds the magnetostatic field between layers which align the magnetizations antiparallel to each other. In such a case, the saturation field can be increased. The dipole–dipole interaction between layers can turn the easy axis from an in-plane direction to the direction parallel to nanowire axis, as has actually been observed for nanowires with disk-shaped magnetic layers and for $\text{Ni}_{80}\text{Fe}_{20}$ (12 nm)/Cu(4 nm) multilayer nanowires reported by Dubois et al. [32]. In the case of CoNi/Cu nanowires, the easy axis remains in the direction perpendicular to the nanowire axis, due to the predominant magnetic anisotropy over dipole–dipole interactions between magnetic layers. The field exerted on a magnetic layer by the dipole–dipole interaction with the adjacent magnetic layers can be estimated using $H_{\text{Dipole}} = m/4\pi r^3$, where m is the dipole moment and r is the distance from the center point of the dipole to a point

that lies on the line which crosses the center point of the dipole and is perpendicular to the dipole axis. In the case of a CoNi layer with $t(\text{CoNi}) = 12$ nm, the dipolar field from the neighboring CoNi layers under a magnetic field applied perpendicular to the nanowire is ~ 2500 Oe. This dipolar field exerts in the direction opposite to the external field so that it reduces the effective magnetic field. This consistently explains the result that the saturation field tends to be larger than that without the dipole interaction when the field is applied perpendicular to the nanowires.

3.4. Coherent rotation and curling modes of magnetization reversal

3.4.1. Magnetization reversal in coherent rotation and curling

As described in Section 1, magnetization reversal can be explained by minimization of the total energy of the system. In general, magnetization measured under a magnetic field is given for the lowest-energy state of the system, and magnetization reversal occurs such that the energy product is minimized by lowering the coercivity [33]. Coercivity varies with many factors such as the shape, crystal structure, and the relative direction between the sample and the external magnetic field. In the case of magnetic nanowires, the magnetization reversal process and coercivity may sensitively change with the angle between the field and the nanowire axis. The angular dependence of coercivity can be closely correlated to the magnetization reversal; different reversal modes are expected to show different trends in the angular dependence of coercivity. For a prolate spheroid, the angular dependence of the coercivity can be calculated for coherent rotation using the classical Stoner–Wohlfarth (SW) model [17]. It has been shown [33] that the normalized coercivity h_c for coherent rotation decreases rapidly with increasing angle ϕ between the field and the easy axis of the magnet. For a prolate spheroid, the angular dependence of h_c for a curling mode can be calculated using the Aharoni's theory [34]. Upon increasing the angle ϕ [33] between the field and easy axis, the value of h_c for curling gradually increases for smaller ϕ while it rapidly increases at larger ϕ . When the angular dependence of coercivity for coherent rotation is compared with that for curling, it has been shown that the coercivity for curling is smaller than that for coherent rotation at smaller ϕ , while it is larger for coherent rotation at larger ϕ [33]. Although these calculations have assumed a prolate spheroid with infinite length, the model is applicable for semiquantitative analysis of a nanowire system with finite length.

3.4.2. Magnetization reversal in CoNi/Cu nanowires with rod-shaped CoNi layers

As described above, magnetization reversal in nanoscale magnets can be explained by analyzing the dependence of coercivity H_c on the angle ϕ between the direction of the applied field and the easy axis. To gain insights into the

reversal in CoNi/Cu nanowires with rod-shaped CoNi layers, the values for H_c have been extracted from hysteresis loops measured for the nanowires and plotted as a function of ϕ . Figs. 5(a) and (b) represent the variation of H_c with changing ϕ for CoNi/Cu nanowire samples with $t(\text{CoNi}) = 7.5$ and 1.0 μm respectively. As described in Section 3.2, the easy axis of these nanowires lies in the direction parallel to the nanowire axis so that $\phi = \theta$ in this case. A slight increase in H_c has been observed with increasing ϕ from 0° to 45° (see Fig. 5), indicating that magnetization reversal in CoNi layers occurs in a curling mode. When ϕ is further increased from 45° to 90° , H_c decreases swiftly and reaches a minimum at around $\phi = 90^\circ$, due to a change in the magnetization reversal from a curling to coherent rotation mode at around $\phi = 45^\circ$.

In general, coercivity H_c of well-aligned fine particle systems depends on the measurement angle ϕ ; at low angles incoherent reversal modes such as curling tend to give lower H_c , while at high angles coherent rotation gives lower

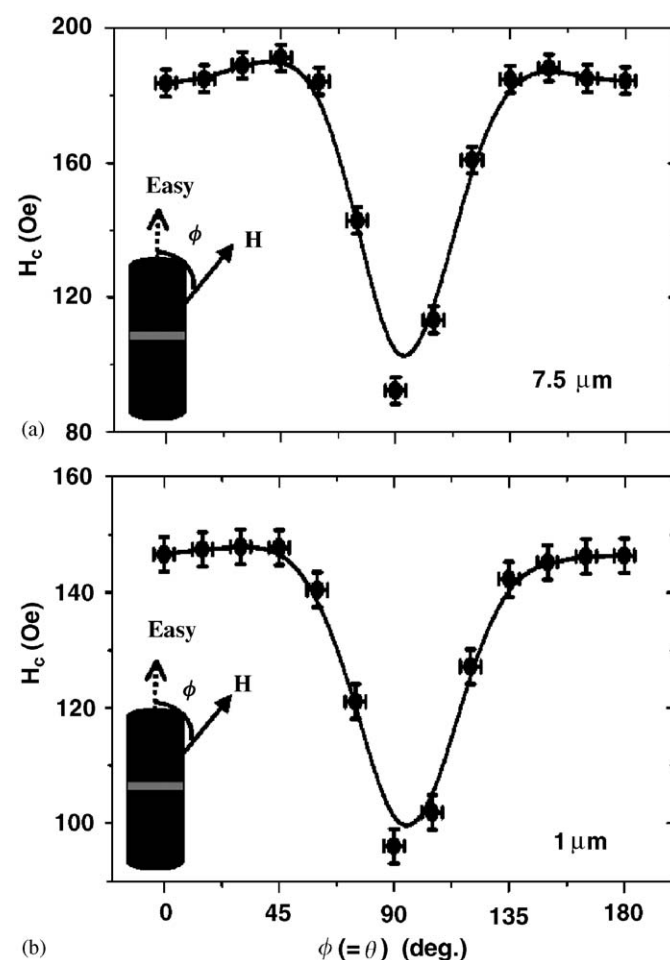


Fig. 5. Coercivity plotted as a function of the angle ϕ between external field and easy axis for CoNi/Cu nanowire samples with (a) $t(\text{Cu}) = 4.2$ nm and $t(\text{CoNi}) = 7.5$ μm and (b) $t(\text{Cu}) = 4.2$ nm and $t(\text{CoNi}) = 1$ μm . The solid curves in (a) and (b) are guides to the eyes. Since the rod-shaped magnetic layers have an easy axis along the nanowire axis, $\phi = \theta$, where θ is the angle between field and nanowire axis.

H_c . Accordingly, incoherent reversal is likely to occur at low ϕ , and coherent rotation at high ϕ . Indeed, the results obtained for the CoNi/Cu multilayer nanowire system suggest that magnetization reversal occurs by curling for $0^\circ < \phi < 45^\circ$ and by coherent rotation for $45^\circ < \phi < 90^\circ$. Han et al. [15] and Goolaup et al. [16] have also reported similar results on single-element magnetic nanowires, showing that curling reversal is present for smaller ϕ and coherent rotation at larger ϕ . It is hereby deduced that multilayer nanowires with rod-shaped magnetic layers show a reversal behavior similar to that of single element nanowires.

In general, coherent rotation and curling reversal models are applicable to magnetic objects smaller than the critical size r_{sd} for single domain particle. On the other hand, for objects larger than r_{sd} , a multidomain state becomes more favorable in order to minimize the magnetostatic energy E_{ms} of the system. In a multidomain system, magnetization reversal involves domain wall motion and pertinent spin rotation within each domain. We have assessed the reversal in multilayer nanowires with rod-shaped CoNi layers using the classical theory for single-domain to multidomain transition [18,33]. For a prolate spheroid, the critical radius r_{sd} for the short axis for the transition from single-domain to multidomain is given by

$$r_{sd} = \sqrt{\frac{6A}{N_c M_s^2} \left[\ln\left(\frac{4r_{sd}}{a} - 1\right) \right]}, \quad (1)$$

where A is the exchange stiffness constant (erg/cm), N_c the demagnetizing factor for the long axis, M_s the saturation magnetization (emu/cm³), and a the lattice constant (cm). Apparently, r_{sd} decreases with decreasing aspect ratio t/d because of the increase in N_c . The value of A for most ferromagnetic metals is in the range 1×10^{-6} – 2×10^{-6} erg/cm [33]. For CoNi, A is taken as 1.5×10^{-6} erg/cm. When $t/d = (7.5 \mu\text{m})/(250 \text{ nm}) = 30$, $N_c = 0.043$ in CGS units. Using these values, one obtains $r_{sd} \sim 420$ nm. Since the radius of the nanowires $d/2$ (~ 125 nm) is smaller than the critical radius, i.e. $r_{sd} > d/2$, the multilayer nanowires should be in a single-domain state. Similarly, when $t/d = (1 \mu\text{m})/(250 \text{ nm}) = 4$, $N_c = 0.948$, that gives $r_{sd} = 80$ nm. In this case, the critical radius is fairly comparable to the actual radius of the nanowires $d/2$ (~ 125 nm); the nanowires should be in the transition region between single-domain and multidomain states. However, the actual data for both $t(\text{CoNi}) = 7.5 \mu\text{m}$ and $1 \mu\text{m}$ show a very similar trend in the angular dependence of H_c (see Figs. 5(a) and 5(b)), indicating that reversal for these samples is of the same type. The observed similarity can be explained by considering dipole–dipole interactions between adjacent magnetic layers in each nanowire. The dipole–dipole interactions tend to align the magnetization of the rod-shaped layer along the nanowire axis with different poles facing each other so that the magnetic behavior of the multilayer nanowires is similar to that of single-element nanowires with large values for t/d and r_{sd} .

3.4.3. Magnetization reversal in CoNi/Cu nanowires with disk-shaped CoNi layers

The thickness of disk-shaped CoNi layers in multilayer nanowires ranges from $t(\text{CoNi}) = 17$ nm to 6.8 nm, which is much smaller than r_{sd} . In this case, reversal by coherent rotation or curling should be considered to account for the magnetization behavior. As described in Section 3.4.1, coercivity H_c increases for curling with increasing angle ϕ between the directions of the applied field and the easy axis, while H_c decreases with ϕ for coherent rotation. As described in Section 3.2, the easy axis for nanowires with disk-shaped CoNi layers lies in a direction perpendicular to the nanowire axis. In this case, H_c decreases with increasing ϕ (see Figs. 6(a) and (b) for $t(\text{CoNi}) = 12$ and 6.8 nm, respectively), indicating that coherent rotation occurs in the CoNi layers. As described in Section 1, reversal can be explained by energy minimization of the system, which takes into account both the exchange energy E_{ex} and magnetostatic energy E_{ms} . For very small $t(\text{CoNi})$, coherent rotation is more stable than curling because it

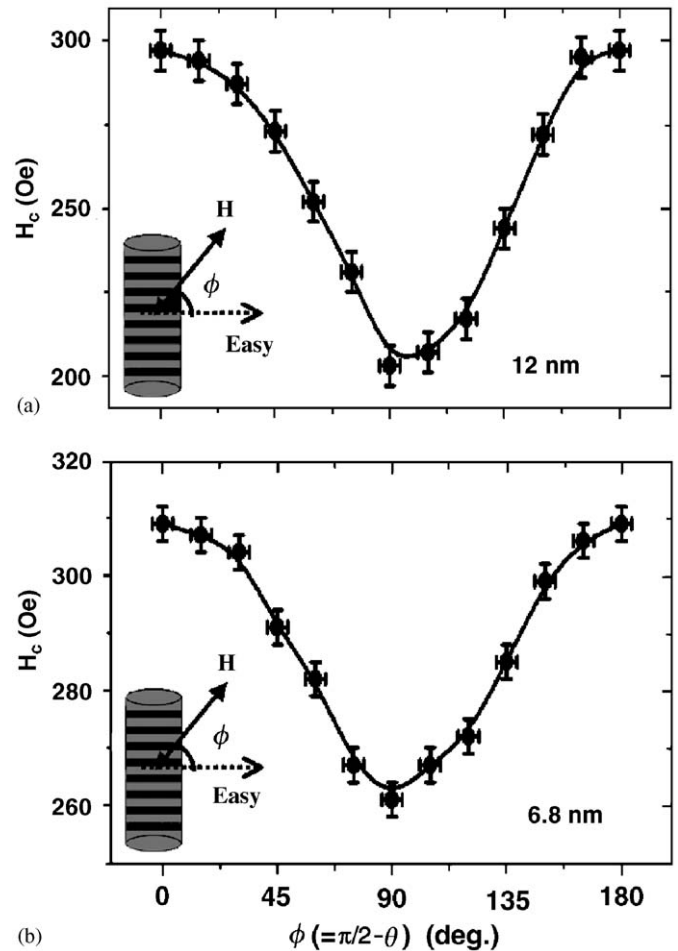


Fig. 6. Coercivity plotted as a function of the angle ϕ between external field and easy axis for CoNi/Cu nanowire samples with (a) $t(\text{Cu}) = 4.2$ nm and $t(\text{CoNi}) = 12$ nm and (b) $t(\text{Cu}) = 4.2$ nm and $t(\text{CoNi}) = 6.8$ nm. The solid curves in (a) and (b) are guides to the eyes. Since the disk-shaped magnetic layers have an easy axis perpendicular to the nanowire axis, $\phi = \pi/2 - \theta$, where θ is the angle between field and nanowire axis.

minimizes E_{ex} . In general, the exchange energy E_{ex} exerted between spins is given by $E_{\text{ex}} = nJ_{\text{ex}}S^2\Phi^2$, where n is the density of spins, J_{ex} the exchange integral, S the spin quantum number, and Φ the angle between spins. All spins in coherent rotation remain parallel so that $\Phi = 0$, i.e. $E_{\text{ex}} = 0$, while spins in curling are distributed in a curling pattern so that $\Phi \neq 0$, i.e. $E_{\text{ex}} \neq 0$. The difference in E_{ex} between coherent rotation and curling is therefore given by $E_{\text{ex}} = nJ_{\text{ex}}S^2\Phi^2$. The magnetostatic energy E_{ms} associated with shape anisotropy can be expressed as $E_{\text{ms}} = 2\pi M^2$ for a disk-shaped magnet with demagnetization factor of 4π for the short axis (i.e. in the thickness direction). For a rough estimation, $E_{\text{ex}} < E_{\text{ms}}$ for $0^\circ < \Phi < 5^\circ$ and $E_{\text{ex}} > E_{\text{ms}}$ for $\Phi > 5^\circ$. Coherent rotation is thus more favorable since the spins are parallel to each other, minimizing E_{ex} .

A transition from coherent rotation to curling as observed for rod-shaped CoNi layers has not been observed for disk-shaped CoNi layers at low angles ϕ , which can be explained by the following two factors. Firstly, the exchange energy E_{ex} for disk-shaped CoNi layers is larger than the value for rod-shaped CoNi layers. In this case, E_{ex} could indeed be more significant than magnetostatic energy E_{ms} even at lower angles ϕ . Secondly, the CoNi layers are not perfectly flat but rather in a wavy shape. When such waviness exists in multilayer nanowires, modulation of the layer interfaces can significantly change the magnetic behavior particularly when $t(\text{CoNi})$ is small [5]. If the modulation is not uniform among the layers, it may result in a variation of the layer thickness. Such a variation in layer thickness tends to increase the distribution of the easy axis among CoNi layers, which results in coherent rotation of the overall reversal in the sample at low angles, although some CoNi layers may locally exist reversal in curling mode.

Disk-shaped magnetic objects are often approximated as oblate spheroids [17]. In coherent rotation an oblate spheroid should show no hysteresis, meaning zero coercivity, but a hysteresis was indeed observed in our case. So the disk-shaped magnetic layer cannot be simply approximated as an oblate spheroid. There are two possible factors that cause the deviation from the model. Firstly, the magnetic layers are not perfectly flat but rather wavy so that the oblate spheroid is not the most suitable model for their shape. Secondly, relatively strong dipole–dipole interactions may exist between adjacent magnetic layers in each nanowire, as described above. Magnetization reversal for disk-shaped magnetic layers in multilayer nanowires can be modulated by such a dipole–dipole interaction between the layers.

4. Conclusion

We have shown that the magnetization reversal mode for CoNi/Cu multilayer nanowires depends on the magnetic layer thickness. Although the magnetic behavior of the CoNi/Cu multilayer nanowires is complicated due to the existence of dipole–dipole couplings between nanowires

and between the adjacent CoNi layers in each nanowire, their reversal mechanism can be qualitatively described by coherent-rotation and curling mode. The reversal for nanowires with thin disk-shaped CoNi layers (nanometer thickness) is of coherent rotation type. In contrast, the reversal for long rod-shaped CoNi layers (micrometer thickness) can be consistently explained by a curling mode when the angle between the easy axis and applied field is lower than 45° , while by coherent rotation when the angle is higher than 45° . Although the dipole–dipole interactions between nanowires do not seem to significantly affect the reversal process, the interactions between adjacent magnetic layers in each nanowire appear to modulate the magnetic behavior. When the magnetic layers in nanowires are in a disk shape, the interactions between the layers tend to align their magnetization along the layer direction antiparallel to each other to give a higher saturation field than that of isolated disk-shaped magnetic objects. When the magnetic layers are in a rod shape, the interactions between the layers tend to align their magnetization along the nanowire axis with different poles facing each other, thus the magnetic layers have a magnetization reversal behavior similar to that of single-element nanowires. The experimental findings in this work are believed to help understand the complicated magnetic behavior of nanoscale multilayer systems and provide additional insights into theoretical modeling of such systems.

Acknowledgments

This work was supported by the seed grant of Rensselaer Polytechnic Institute and the National Science Foundation Award no. 05 06 738. We thank Tom Parker and Dexian Ye for their assistance in XRD and SEM measurements.

References

- [1] L. Piraux, J.M. George, J.F. Despres, C. Leroy, E. Ferain, R. Legras, K. Ounadjela, *Appl. Phys. Lett.* 65 (1994) 2484.
- [2] K. Liu, K. Nagodawithana, P.C. Searson, C.L. Chien, *Phys. Rev. B* 51 (1995) 7381.
- [3] W. Schwarzacher, K. Attenborough, A. Michel, G. Nabyouni, J.P. Meier, *J. Magn. Mater.* 165 (1997) 23.
- [4] P.R. Evans, G. Yi, W. Schwarzacher, *Appl. Phys. Lett.* 76 (2000) 481.
- [5] X.-T. Tang, G.-C. Wang, M. Shima, *J. Appl. Phys.* 99 (2006) 033906.
- [6] A. Thiaville, J.M. García, J. Miltat, *J. Magn. Mater.* 242 (2002) 1061.
- [7] K.Yu. Guslienko, V. Novosad, Y. Otani, H. Shima, K. Fukamichi, *Phys. Rev. B* 65 (2002) 24414.
- [8] S.L. Whittenburg, N. Dao, C.A. Ross, *Physica B* 306 (2001) 44.
- [9] H. Qu, J.Y. Li, *Phys. Rev. B* 68 (2003) 212402.
- [10] N. Dao, S.L. Whittenburg, *IEEE Trans. Magn.* 39 (2003) 2525.
- [11] B. Raquet, B. Mamy, J.C. Ousset, *Phys. Rev. B* 54 (1996) 4128.
- [12] K.Yu. Guslienko, V. Novosad, Y. Otani, H. Shima, K. Fukamichi, *Phys. Rev. B* 65 (2001) 024414.
- [13] E.Y. Vedmedenko, N. Mikuszeit, H.P. Oepen, R. Wiesendanger, *Phys. Rev. Lett.* 95 (2005) 207202.
- [14] H. Niedoba, M. Labrune, *Eur. Phys. J. B* 47 (2005) 467.
- [15] G.C. Han, B.Y. Zong, P. Luo, Y.H. Wu, *J. Appl. Phys.* 93 (2003) 9202.

- [16] S. Goolaup, N. Singh, A.O. Adeyeye, V. Ng, M.B.A. Jalil, *Eur. Phys. J. B* 44 (2005) 259.
- [17] E.C. Stoner, E.P. Wohlfarth, *Phil. Trans. R. Soc. Lond. A* 240 (1948) 599.
- [18] E.H. Frei, S. Shtrikman, D. Treves, *Phys. Rev.* 106 (1957) 446.
- [19] W.F. Brown, *Phys. Rev.* 105 (1957) 1479.
- [20] S. Okamoto, O. Kitakami, N. Kikuchi, T. Miyazaki, Y. Shimada, *Phys. Rev. B* 67 (2003) 094422.
- [21] W. Schwarzacher, D.S. Lashmore, *IEEE Trans. Magn.* 32 (1996) 3133.
- [22] M. Shima, L. Salamanca-Riba, T.P. Moffat, R.D. McMichael, L.J. Swartzendruber, *J. Appl. Phys.* 84 (1998) 1504.
- [23] G.J. Strijkers, J.H.J. Dalderop, M.A.A. Broeksteeg, H.J.M. Swagten, W.J.M. de Jonge, *J. Appl. Phys.* 86 (1999) 5141.
- [24] D.J. Sellmyer, M. Zheng, R. Skomski, *J. Phys.: Condens. Matter* 13 (2001) R433.
- [25] H. Zeng, M. Zheng, R. Skomski, D.J. Sellmyer, Y. Liu, L. Menon, S. Bandyopadhyay, *J. Appl. Phys.* 87 (2000) 4718.
- [26] M. Zheng, L. Menon, H. Zeng, Y. Liu, S. Bandyopadhyay, R.D. Kirby, D.J. Sellmyer, *Phys. Rev. B.* 62 (2000) 12282.
- [27] L. Piraux, S. Dubois, E. Ferain, R. Legras, K. Ounadjela, J.M. George, J.L. Maurice, A. Fert, *J. Magn. Magn. Mater.* 165 (1997) 352.
- [28] R. Ferré, K. Ounadjela, J.M. George, L. Piraux, S. Dubois, *Phys. Rev. B* 56 (1997) 14066.
- [29] A. Kazadi Mukenga Bantu, J. Rivas, G. Zaragoza, M.A. López-Quintela, M.C. Blanco, *J. Appl. Phys.* 89 (2001) 3393.
- [30] Q.F. Zhan, J.H. Gao, Y.Q. Liang, N.L. Di, Z.H. Cheng, *Phys. Rev. B.* 72 (2005) 024428.
- [31] M. Chen, P.C. Searson, C.L. Chien, *J. Appl. Phys.* 93 (2003) 8253.
- [32] S. Dubois, C. Marchal, J.M. Beuken, L. Piraux, J.L. Duvail, A. Fert, J.M. George, J.L. Maurice, *Appl. Phys. Lett.* 70 (1997) 396.
- [33] L. Sun, Y. Hao, C.-L. Chien, P.C. Searson, *IBM J. Res. Dev.* 49 (1) (2005) 79.
- [34] A. Aharoni, *J. Appl. Phys.* 82 (1997) 1281.